A model of residual currents and pollutant transport in the Arabian Gulf

R. W. Lardner†, W. J. Lehr, R. J. Fraga, and M. A. Sarhan

Department of Mathematical Sciences, King Fahd University of Petroleum & Minerals, Dhahran, Saudi Arabia
(Received April 1987; revised October 1987)

A pollutant transport model is presented for the Arabian Gulf, with particular relevance to the portion of the Gulf adjacent to the coast of Saudi Arabia. The model has been developed specifically for oil spill simulations, but it can be adapted to other pollutants. The residual currents in this part of the Gulf are dominated by wind-forcing, and part of the model consists of a computation of the mean wind-driven currents for each month. This is achieved by first solving the shallow-water equations (using a finite difference algorithm) for the depth-averaged velocities, and then solving the momentum equations for the vertical velocity profiles. The pollutant transport part of the model includes surface spreading of the slick, evaporation and dispersion into the water column, convection, and both horizontal and vertical dispersion of the pollutant plume. The model is applied to the simulation of a 5000-barrel surface spill in the Marjan offshore oil field.

Keywords: residual current, pollutant transport, oil spill, (Arabian) Gulf, convection-diffusion model

Introduction

The hazards of pollution in the Arabian Gulf have increased significantly in the last two decades as a result of the high levels of production and transportation of petroleum and also of the growing industrialization and urban development around its shores. The purpose of this paper is to describe a mathematical model of the convection and dispersion of pollutants in the areas of the Gulf adjacent to the Saudi Arabian coastline.

In order to simulate the behavior of pollutants, it is essential to have a knowledge of the currents in the area. As far as long-term convection of pollutants is concerned, the residual currents* are generally more significant than the cyclic tidal currents or the transient flows induced by storms. The second and third sections therefore are devoted to a description of a model of the residual currents in the Gulf with particular emphasis on the areas in proximity to the Saudi Arabian coastline. Then with the current model as one of its inputs, the fourth section is concerned with a model for the convection and diffusion of pollutants.

Residual flow in the Gulf has been attributed to two principal factors: wind-forcing, which, coupled with Coriolis effects, generates a net anticlockwise circulation; and the effect of horizontal density gradients, which are generated and sustained by evaporative losses and radiative heat transfer and, to a lesser extent, by freshwater inflow at the head of the Gulf. The relative importance of these two mechanisms has been the subject of considerable debate. In Ref. 1 Hughes and Hunter argued that wind-driven currents based on Ekman dynamics contributed in a major way to the residual currents, but, more recently, Hunter[2] concluded that the circulation is probably dominated by density-driven currents geostrophically balanced across the Gulf and frictionally balanced in the direction of flow. Galt *et*

* For our purposes the "residual" current may be identified with the monthly average current. This current varies somewhat on a seasonal timescale but is relatively constant over periods of 10 or 20 days.

† Present address: Simon Fraser University, Burnaby, British Columbia, Canada

al.[3] agree with this assessment in the southern half of the Gulf, but conclude that wind-driven circulation plus the effect of freshwater inflow dominate in the northern half.

In earlier papers[4–6] the authors estimated the density-driven and wind-driven currents in the Gulf and compared these estimates with the empirical values derived by Hunter[2] from ship-drift data. The density-driven component of the flow is sufficient on its own to explain Hunter's empirical values within the Strait of Hormuz itself. As one moves into the Gulf, the density-driven flow velocity decreases and the wind-driven flow increases in significance; after about 100 km from the Strait the wind-driven flow is more important than the density-driven flow. In the northern half of the Gulf, the inflow of freshwater from the Shatt-al-Arab produces rather small currents except in the immediate vicinity of the Shatt itself, and with this exception the flow is entirely dominated by the wind-driven component. In particular, this is true of the areas adjacent to the Saudi Arabian coastline, with which this paper is principally concerned.

The annual average wind-driven flow in the northern Gulf involves a surface velocity that is uniformly toward the southeast, except where it is forced to deviate by the coastline. The surface velocity is between 0.1 and 0.3 m/s over most of this region, which is consistent with drift-buoy measurements[7] as well as with observations of the movements of the Nowruz oil spill.[3] However, at subsurface levels, particularly in the central part of the northern Gulf, there is a return flow towards the northwest, the flow velocity being generally less than 0.1 m/s. This subsurface flow leads, as we shall see, to a significant and important difference between the positions of a surface oil slick and its associated subsurface pollutant plume. It also has significant implications regarding the dumping of industrial waste from underwater outfalls.

For the pollution transport model we decided to use oil as the prototype pollutant for two reasons. The first is that oil is a more complex pollutant than other possible choices, insofar as it forms a surface slick as well as a subsurface dispersed plume. The spreading, evaporation, and surface dispersion of the slick add extra complications that would not be present for a model of a passive pollutant that is simply dispersed through the water column. The second reason for choosing oil is simply that it is presently the most widespread pollutant in the Gulf region.

As an illustration of the use of the model, the paper contains the results of a simulation of a 5000-barrel surface oil spill in the Marjan oil field. The distribution of the surface slick and the subsurface plume are presented at certain intervals of time following the spill as well as the amounts of evaporated and grounded oil.

Wind-driven circulation in the gulf

Winds in the Gulf region blow predominantly from the sector between the north and west and so generate a net shear stress acting roughly from the northwest. The induced currents have been computed by incorporating this stress into the shallow-water equations. These equations were solved by a finite difference algorithm based on Leendertse's scheme.[8–10] The vertical profiles of the current were then computed using the method of Lardner and Cekirge.[11]

The depth-average shallow-water equations are as follows:

$$\frac{\partial \bar{u}}{\partial t} + \bar{u}\frac{\partial \bar{u}}{\partial x} + \bar{v}\frac{\partial \bar{u}}{\partial y} = f\bar{v} - g\frac{\partial \zeta}{\partial x} + \frac{1}{\rho H}(-\tau_x^b + \tau_x^s) \tag{2}$$

$$\frac{\partial \bar{v}}{\partial t} + \bar{u}\frac{\partial \bar{v}}{\partial x} + \bar{v}\frac{\partial \bar{v}}{\partial y} = -f\bar{u} - g\frac{\partial \zeta}{\partial y} + \frac{1}{\rho H}(-\tau_y^b + \tau_y^s) \tag{3}$$

where ζ = surface height above xy-plane
H = total depth of water = $h + \zeta$
h = depth of bottom below xy-plane
$(\bar{u}, \bar{v})$ = depth-averaged components of velocity in x and y directions
g = acceleration due to gravity
f = Coriolis parameter = $2\Omega \sin \phi$ (where ϕ = latitude and Ω = angular velocity of the earth)
ρ = water density
(τ_x^s, τ_y^s) = components of surface shear stress
(τ_x^b, τ_y^b) = components of bottom friction stress

The bottom shear stresses are taken to be quadratic in the velocities, given by

$$(\tau_x^b, \tau_y^b) = \frac{g\rho}{c^2}(\bar{u}^2 + \bar{v}^2)^{1/2}(\bar{u}, \bar{v}) \tag{4}$$

where c is the Chezy coefficient. In an earlier model of tidal flow in the Gulf[10] c was taken to have the form

$$c = c_1 \log(c_2 H + c_3) \tag{5}$$

The values $c_1 = 25.0$, $c_2 = c_3 = 1.0$ were found to give the best fit of the observed tidal ranges and phases. The same Chezy coefficients are used in the present work. (MKS units are used throughout.)

The surface shear stress $\boldsymbol{\tau}^s = (\tau_x^s, \tau_y^s)$ produced by the wind is generally taken to be given by the formula

$$\boldsymbol{\tau}^s = \gamma \rho_a w^2 (d_x, d_y) \tag{6}$$

where γ = dimensionless drag coefficient
ρ_a = density of air
w = wind speed
$\mathbf{d} = (d_x, d_y)$ = unit vector in the direction of the wind

Over the years a number of expressions have been proposed for the drag coefficient γ. A comparison of several of these is given by Mathison and Johansen,[12] who found that with one exception the various expressions all result in similar values of surface stress. Following these authors, we have adopted the formula of Lystad and Martinsen:[13]

$$\gamma = \begin{cases} a + bw & \text{for } w < w_1 \\ c & \text{for } w \geq w_1 \end{cases} \quad (7)$$

with $a = 0.00089$, $b = 0.00013$, $c = 0.0028$, $w_1 = 15$ m/s.

We assume that for any given wind direction and for any month the wind speed in exponentially distributed. Then by (7) the mean value of γw^2 for any direction is given by

$$\langle \gamma w^2 \rangle = 2\bar{w}^2\{a + 3b\bar{w} + e^{-\beta} \times [(c - a - 3b\bar{w})(1 + \beta + \beta^2) - \tfrac{1}{2}b\bar{w}\beta^3]\} \quad (8)$$

where $\bar{w}$ is the monthly mean wind speed for the direction in question and $\beta = w_1/\bar{w}$.

In order to compute the average circulation for each month of the year, meteorological data prepared by the Naval Oceanography Command Detachment[14] were used to determine on a monthly basis the average speeds of the winds from each of the eight cardinal directions and the percentage of time for which these eight winds blew. An average effective wind velocity vector $\bar{\mathbf{w}}$ was then computed from the formula

$$|\bar{\mathbf{w}}|\bar{\mathbf{w}} = \frac{1}{c}\sum_{i=1}^{8}\left(\frac{a_i}{100}\right)\langle \gamma w^2 \rangle_i \mathbf{d}_i \quad (9)$$

where i indexes each of the cardinal directions

a_i = percent of the time the wind blows from direction i

$\mathbf{d}_i$ = unit vector from direction i

and $\langle \gamma w^2 \rangle_i$ is obtained from equation (8) for each direction i. The normalization constant c in equation (9) is chosen for convenience as the maximum value of the drag coefficient (7).

By combining equations (6) and (9), we obtain the mean surface shear stress vector

$$\langle \boldsymbol{\tau}^s \rangle = c\rho_a|\bar{\mathbf{w}}|\bar{\mathbf{w}} \quad (10)$$

The computed values of the magnitude of $\bar{\mathbf{w}}$ and its geographical direction (in degrees east of north) are given in *Table 1*. The average effective wind velocity is approximately from the northwest throughout the year with maximum deviations of +13° and −18°. The mean effective wind speed varies between a minimum of 3.0 m/s in August and a maximum of 5.5 m/s in February.

Since the mean wind direction is more or less constant throughout the year, the resulting currents turn out to be qualitatively similar for all months, the difference from one month to another consisting only in the magnitude of the current vectors. The last column of *Table 1* gives the ratio of the magnitude of the mean surface stress (10) for each month to the corresponding magnitude for the year as a whole. To quite a good approximation, the flow velocities for any month can be obtained from the annual average values given below and in the next section by multiplying by the appropriate ratio from this column. It can be seen that the currents are above average during the winter and summer shamal periods of January–March and May–June and are below average during August–October.

The dynamical computational scheme obtained from equations (1)–(3) was run using the mean wind stress (10) for each period (i.e., for each month or for the whole year). Starting with initially flat conditions, each computation was run until approximately stable currents were obtained (which occurs after about 72 h of real time).

The resulting velocities for the annual average wind stress are shown in *Figure 1* for the Gulf as a whole and in *Figure 2* in finer detail for a strip of width approximately 150 km parallel to the Saudi Arabian coastline.

From *Figure 1* we see that the main features of the average annual circulation in the northern Gulf are flows of magnitude 0.1–0.15 m/s southeastward along both the Saudi and Iranian coasts, across the northern coast of Bahrain, and round the Qatar peninsula. In the central area of the northern Gulf there is a weak return flow of magnitude 0.03–0.06 m/s toward the

Table 1 Average effective wind velocity vectors (m/s). The mean surface shear stress is given by Equation (10). The last column is the ratio of shear stress magnitude to its annual average value

Month	Wind velocity	Wind direction	Ratio
Jan.	5.324	141.7	1.42
Feb.	5.487	131.7	1.51
Mar.	5.066	132.5	1.28
Apr.	4.483	128.5	1.01
May	4.724	118.5	1.12
Jun.	4.892	127.7	1.20
Jul.	3.892	122.8	0.76
Aug.	3.000	126.3	0.45
Sep.	3.465	132.8	0.60
Oct.	3.296	143.4	0.54
Nov.	4.689	147.8	1.10
Dec.	4.784	135.9	1.14
Annual	4.471	132.7	—

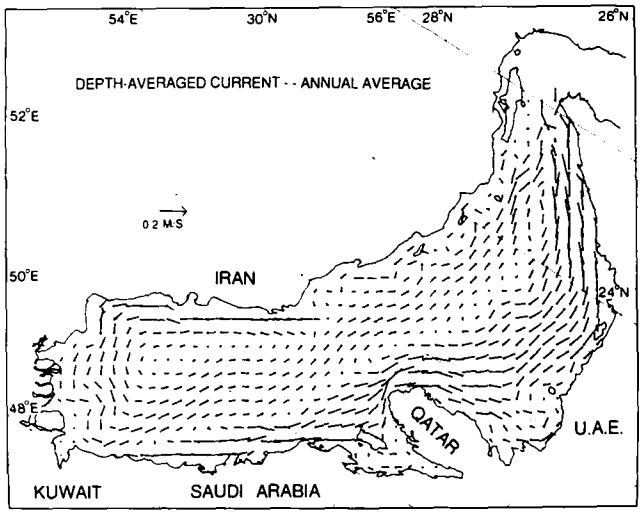

Figure 1 Depth-averaged wind-driven current in the Gulf with annual average winds

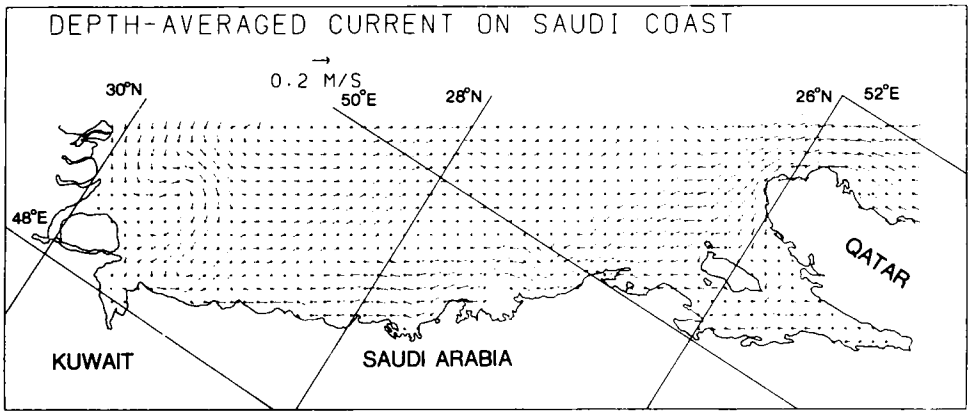

Figure 2 Depth-averaged annual average current near the Saudi coast

northwest. This return flow has a separation point on the northern coast in the vicinity of Kuwait. These features are also clear in *Figure 2*.

In the southern Gulf the flow around the Qatar peninsula continues along the Emirates coast with velocities in the range 0.1–0.17 m/s. In the Strait of Hormuz there is outward flow on the southern (Emirates) side and return inward flow on the northern (Iranian) side. The band of return flow is wider and weaker than the outward flow, the velocities being 0.09–0.14 m/s within the Strait and decreasing to 0.07 at a position 200 km inside the Gulf.

The results in *Figure 1* are consistent with those computed earlier by Galt *et al.*,[3] using a simplified model. The return flow to the northwest predicted to occur in the central portion of the northern Gulf has been a curious anomaly since the publication of these results because it is not consistent with the observed movement of oil slicks[3] or with recent drift-buoy studies.[7] As we shall show in the next section, the reason for this discrepancy rests in the difference between the depth-averaged and surface flows in this region.

Vertical current profiles

By a method developed by Lardner and Cekirge,[11] it is possible to construct vertical profiles of the velocity through the water column using the output from the depth-averaged computation.

The horizontal momentum equations for a steady flow take the form

$$\frac{\partial}{\partial z}\left(N\frac{\partial u}{\partial z}\right) + fv - g\frac{\partial \zeta}{\partial x} = 0$$
$$\frac{\partial}{\partial z}\left(N\frac{\partial v}{\partial z}\right) - fu - g\frac{\partial \zeta}{\partial y} = 0 \qquad (11)$$

In these equations we have neglected the advective terms, which can be shown to be relatively insignificant in the problems under consideration. We use $u(x,y,z)$, $v(x,y,z)$ to denote the horizontal velocity components at the point (x,y,z), z being a vertical axis with the bottom at $z = -h$ and the free surface at $z = \zeta$. N is the vertical eddy velocity, which may depend on (x,y,z).

Equations (11) form a system of two second-order ordinary differential equations for the z-dependence of u and v. The terms $\partial\zeta/\partial x$ and $\partial\zeta/\partial y$ can be obtained from the depth-averaged computation, so these equations may readily be solved by a standard numerical integration routine. (In practice, a fourth-order Runge-Kutta routine was used.) Two of the required boundary conditions are taken as the free-surface stress condition

$$\rho N\frac{\partial u}{\partial z} = \tau_x^s \quad \rho N\frac{\partial v}{\partial z} = \tau_y^s \qquad \text{on } z = \zeta \qquad (12)$$

where (τ_x^s, τ_y^s) are given by equation (10). The other two conditions on u and v use the mean velocities,

$$\int_{-h}^{\zeta} u\,dz = (h + \zeta)\bar{u} \qquad \int_{-h}^{\zeta} v\,dz = (h + \zeta)\bar{v} \qquad (13)$$

where again $\bar{u}$, $\bar{v}$, and ζ are taken from the depth-averaged computation. The algorithm used is based on a shooting method: the values of u and v at $z = \zeta$ are guessed, so these guesses together with condition (12) form an initial value problem for system (11). The guessed initial data are then adjusted until a final solution is obtained that satisfies conditions (13). (See Ref. 11 for further details.)

The eddy viscosity N was given a constant value over most of the water column. On the basis of a mixing length hypothesis, we would expect N to decrease near the bottom and top surface, and we have allowed N to decrease linearly to the surface value N_s over the top 10 m. Since we are not primarily concerned with exactly modeling the bottom boundary layer, we have not included a corresponding decrease at the bottom. The present algorithm is not suitable for calculating the bottom boundary layer because it uses expression (4) for the bottom friction stresses rather than the more correct expressions involving the actual bottom velocities. This feature was found[11] to make little difference to the surface boundary layer.

The value used for the bulk eddy viscosity was estimated from the Neumann-Pierson formula[15]

$$N = (1.8 \times 10^{-4})w^{5/2} \qquad \text{(MKS units)}$$

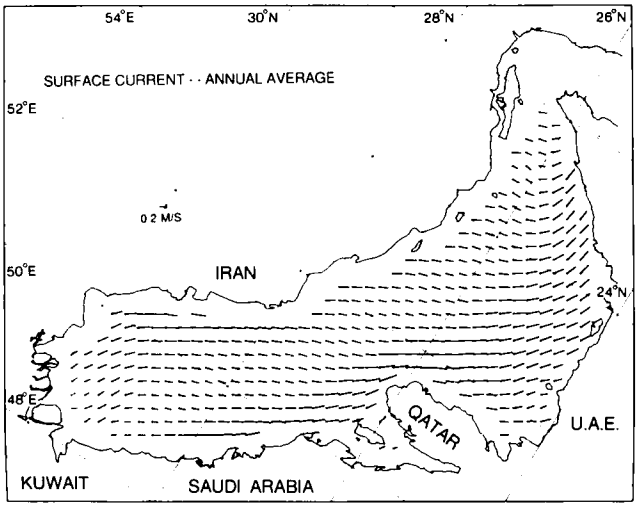

Figure 3 Surface current in the Gulf due to annual average winds

With an average wind speed $w \sim 5$ m/s, we obtain $N \sim 0.01$ m^2/s.

Following Davies,[16] we can estimate the surface eddy viscosity as $N_s = k_0 u_* z_0$, where $k_0 = 0.4$ is von Karman's constant, z_0 is the roughness length (taken as 0.1 m), and u_* is related to the surface shear stress by $\tau^s = \rho u_*^2$. Using estimate (10) for the average shear stress gives $u_* \sim 8 \times 10^{-3}$ m/s and $N_s \sim 0.0003$. This is the value used in the results that follow.

The resulting annual average surface current is shown in *Figure 3* for the Gulf as a whole and in *Figure 4* for the region adjacent to the Saudi Arabian coast. It turns out to be different from the depth-averaged current in *Figures 1* and *2*. The most striking difference is that the northwest-flowing current in the center of the northern Gulf is reversed, and throughout the northern Gulf the surface flow is roughly parallel to the wind direction. The northwest-flowing current exists mainly at the lower levels of the water column, whereas at the surface the flow is toward the southeast, with velocities between 0.1 and 0.3 m/s. In the central part of the northern Gulf this flow is confined to a surface layer of thickness 10–20 m, and beneath this layer a strong reverse flow occurs.

These results help to explain why observations on oil slick movement[3] and on the trajectories of drift buoys[7] do not show the steady northwestward motion in the center of the northern Gulf that is shown by *Figure 1* and by the computed results of Galt and coworkers.[3] The numerical values of the surface currents shown in *Figures 3* and *4*, when corrected for the months in question using the ratios in *Table 1*, are in very reasonable agreement with the drift-buoy observations reported in Ref. 7.

Convection-diffusion model

The most common pollutant in the Gulf is spilled oil with estimates as high as 1.5 million tons spilled annually.[17] Since oil both spreads and moves over the surface, as well as disperses in the water column, it was selected as the demonstration substance to calibrate and illustrate the model. Only slight modification allows the model to be used for passive subsurface pollution studies.

The convection-diffusion model is designed to provide a solution to the general transport equation

$$\frac{\partial \rho}{\partial t} = -\mathbf{V}\cdot\nabla\rho + \nabla\cdot(D\nabla\rho) + S$$

where ρ is the density of the pollutant
$\mathbf{V}$ is the convective velocity of the transporting medium
D is the dispersion tensor
S represents any source or sink terms

For a surface pollutant such as oil there are additional considerations related to surface spreading, which will be discussed later.

When constructing a mathematical analog for simulating mass transport, we can view a physicochemical system such as oil as a continuum of matter or as a large, finite ensemble of small discrete quantities. This latter approach is the basis of the so-called Monte-Carlo method and has been selected for the present

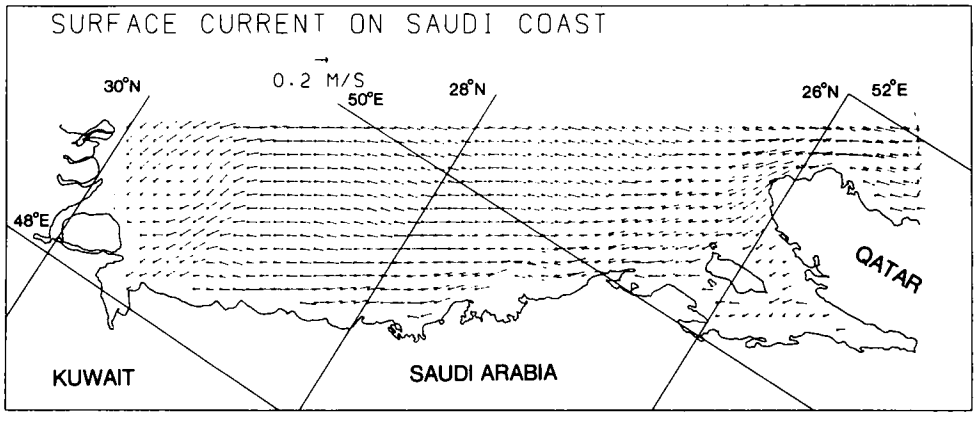

Figure 4 Annual average surface current near the Saudi coast

model, with each Lagrangian element equivalent to one barrel of oil. The barrels are subject to transport by the movement of the surrounding water, dispersion, and surface spreading. The spill site provides a time-varying source of the oil, and the weathering effects on the oil can be considered as sinks, as can also the shorelines where the oil may be deposited. The details of each of these processes are described below.

Surface spreading

The spread of a multicomponent hydrocarbon mixture such as crude oil on the surface of a distinctly different fluid like water is an extremely complicated problem in multiphase fluid dynamics. None of the existing models can be considered to be truly reliable under actual field conditions.[18,19] The most widely used spreading formula is the Fay algorithm,[20] which divides the spreading of oil into three phases, although the middle, gravity-viscous, phase is the most important for practical oil spill simulation. The initial fast phase is simulated in the present model by giving the spill an initial finite radius. Assumptions about the initial thickness, and hence the initial size of the spill, are adopted from Mackay and Leinonen.[21]

Research done on experimental spills in the Arabian Gulf[22] found that a significant improvement was produced in the gravity-viscous phase if a wind factor was included. This modification, therefore, has been adopted for this model. The oil is then assumed to spread as an ellipse with the major axis in the direction of the wind. The area of the ellipse is[22]

$$A = (\pi/4)QR$$

where Q = length of the minor axis
$= 1.7[\rho_w - \rho_0)/\rho_0]^{1/3}V^{1/3}t^{1/4}$
R = length of the major axis
$= Q + 0.03\, w^{4/3}t^{3/4}$
t = time in minutes
ρ_w = water density
ρ_0 = oil density
V = initial volume of spill in barrels
w = wind speed in knots

To simplify the notation given here, the x-axis is taken as oriented in the direction in which the wind is blowing. It is assumed that the slick spreads uniformly insofar as the ratio of the lengths of the major and minor axes of an interior ellipse of particles to those of the boundary ellipse is a constant over time. Then the spreading displacement of an oil particle at the position (x,y) within the slick during a time step dt is given by

$$dx = Sx\,dt \qquad dy = Sy\,dt$$

where $S = (Q^3R'x^2 + R^3Q'y^2)/QR(Q^2x^2 + R^2y^2)$
$Q' = dQ/dt$
$R' = dR/dt$

Weathering

Degradation of the oil slick is represented by breakup of the oil into the water column and by evaporation. (Neglected in the model are such phenomena as dissolution, photooxidation, and emulsification. According to Huang[23] and Mackay and Stiver,[24] these phenomena are of secondary importance during the early period of the spill.)

Mackay and Leinonen,[21] Holmes,[25] and Blaikely *et al.*,[26] found reasonable results for dispersion of the surface oil into the water column by a first-order process where the dispersion constant was a step function of the sea state and hence wind speed. For this model, we have used

$$\frac{1}{V}\left(\frac{dV}{dt}\right)_d = k_d$$

where V = volume of the oil spill
$(dV/dt)_d$ = rate of breakup of the oil into the water column
k_d = dispersion constant

The values of k_d are taken from Mackay and Leinonen:[21]

$k_d = 0.0063$ for $w < 5$ m/s
$= 0.010$ for $5 \le w < 20$ m/s
$= 0.015$ for $w > 20$ m/s

where w is the wind speed. To apply this formula to the individual Lagrangian element, we consider k_d as a probability of dispersion of that element into the water column. A random number of uniform distribution between 0 and 1 is computed for each element. If the number is less than k_d, that element is assumed to have been driven into the water column and will no longer be considered for surface phenomena such as spread or evaporation.

Evaporation is simulated by assuming that the oil can be separated into two components: an evaporative part and a residual part. Parameters to determine the rate and total amount of evaporation are chosen based on the studies of Aravamunden *et al.*[27] If c_i, ρ_i are respectively the fraction and density of the component i ($i = 1, 2$) then

$$c_1 + c_2 = 1 \qquad c_1\rho_1 + c_2\rho_2 = \rho$$

Table 2 gives initial values of these parameters for Arabian light crude and for a typical heavy crude. The evaporative flux k_e is approximated by

$$k_e = k_0 w p_1$$

where k_0 = flux constant
p_1 = partial pressure of the evaporative component $= \dfrac{c_1/m_1}{(c_1/m_1 + c_2/m_2)} P_1$

Table 2 Parameters for the evaporation algorithm. The surface temperature T_s is taken as 25°C, and the ratio of molecular weights m_1/m_2 is taken as 0.67

Oil type	c_1	ρ_1	ρ_2	T_1 (°C)
Light crude	0.66	0.83	0.965	226
Heavy crude	0.60	0.86	1.06	316

Here m_i = molecular weight of component i, and P_i is the vapor pressure at saturation temperature. Aravamunden approximates

$$P_i \approx \exp(-5[(T_i - T_s)/T_s])$$

where T_s is the surface temperature, and values for T_i for light and heavy crude are given in *Table 2*.

Aravamunden's empirical value for the flux constant k_0 was selected to conform to Fay's formula for spreading. Since the authors are using a modification of that formula to accord with results observed in a series of test spills in the Gulf,[18] Aravamunden's value for k_0 has been suitably altered to allow for evaporation to be mostly finished after two days, a phenomenon generally accepted in case studies of oil spills.[27] The value $k_0 = 10^{-9}$ s²/m² is used in the simulation developed here.

Convection and dispersion

All the Lagrangian elements are moved by the surrounding water medium. The current patterns for the region were obtained from the algorithm described in the second and third sections. For purposes of input data to the transport model, the water column was divided into four levels and the currents in each level computed: surface currents, average currents from 0 to 10 m, average currents between 10 and 20 m, and average currents below 20 m.

Dispersion is separated into horizontal and vertical dispersion. Okubo[28] studied the diffusion of contaminants in the upper mixed layer. Based on analysis of these studies, Venkatesh, Sahota, and Rizkalla[29] recommended a horizontal diffusion constant

$$D_h = 10\ \text{m}^2/\text{s}$$

for oil pollution. The authors have used Nihoul's[30] value for the vertical dispersion constant

$$D_v = 10^{-2}\ \text{m}^2/\text{s}$$

The actual model of the dispersion of the individual Lagrangian elements uses the same mathematical approach as Ahlstrom[31] for oil diffusion. The horizontal root mean square distance, d_{rms}, traveled by an average element in time Δt is

$$d_{rms} = \sqrt{4D_h \Delta t}$$

The diffusion step size d for any individual element is generated randomly by

$$d = [R]_0^r$$

Here $[R]_0^r$ represents a random number in the range 0 to r, and r is chosen so that the root mean square of all d values will equal d_{rms}. Since the random-number generator used in the program is designed to return numbers between 0 and 1, and since

$$\left[\int_0^1 d^2\,\mathrm{d}d\right]^{1/2} = \frac{1}{\sqrt{3}}$$

it follows that

$$d = \sqrt{3}\,[R]_0^1 \sqrt{4D_h \Delta t}$$

An approach similar to this is used to select the size of the vertical diffusion step, the result being

$$d_v = \sqrt{3}\,[R]_0^1 \sqrt{2D_v \Delta t}$$

The direction θ of the horizontal diffusion step is randomly selected as $\theta = 2\pi[R]_0^1$ for each element of each time step.

Simulation of a spill in the Marjan oil field

The Marjan oil field is a major offshore oil field in the northeastern part of the Aramco concession area, approximately 28.5°N latitude, 49.5°E longitude. Pipelines connect the field to the Zuluf and Safaniya fields. Although little is known about the ecology of the marine communities in this region, it is near important fishing and shrimp breeding areas.

Potential spills from the field range in size from over 50,000 barrels in the case of a rupture of a 22-inch pipeline between Marjan and Zuluf to less than 100 barrels in the case of a valve leak from a tie-in platform.[32]

The simulated spill that the authors have selected to demonstrate the dispersion model involves a 5000-barrel surface spill, released over a 10-h period in the Marjan field. The oil is assumed to have an API of 32.4, the density of Marjan GOSP-1 oil production. The parameters given in *Table 2* for light crude were used.

Two time scales are selected to study the spill: for the first 72 h, when weathering effects are significant, output is calculated every 2 h. After that, when evaporation and spreading have effectively ceased, the spill changes and movements are calculated at 3-h intervals.

Each Lagrangian element is removed or transported according to the previous formulas for each time step. Surface oil is assumed to stick to any land boundary that it encounters, whereas subsurface elements are assumed to be reflected by any impacted boundary. Since oil near the shore generally gets mixed with sediment and sinks to the bottom, the authors have selected 2 m or less as the depth at which the oil is assumed to be grounded. The density of surface oil that is still spreading can be computed from the evaporation algorithm. Subsurface density is calculated by counting the number of Lagrangian elements in the appropriate water volume. Thus at each time step the size and location of the surface spill are obtained, and the distribution of the subsurface pollutant plume within each of the three layers of water can be calculated.

A record is also maintained of the locations at which the oil impacts the coastline or is grounded in shallow water.

Figures 5 to *7* show the amount of oil that evaporated, dispersed in the water column, and came ashore. As *Figure 5* demonstrates, evaporation is by far the most important process in the weathering of the oil in a high-temperature climate like that of the Gulf. The net 60% loss to evaporation is consistent with the evaporation loss results predicted by the model of Mackay and Leinonen.[21]

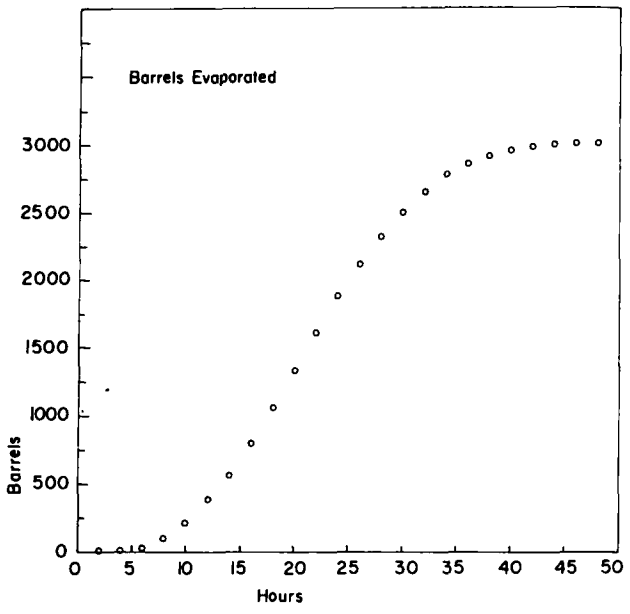

Figure 5 Number of barrels evaporated from the spill as a function of time (hours)

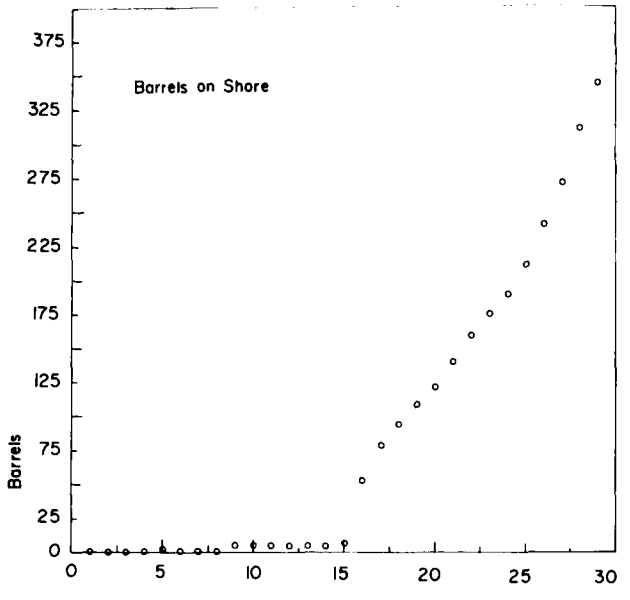

Figure 7 Number of barrels that have hit the shoreline as a function of time (days)

Figure 6 shows the number of barrels dispersed in the water column. It can be seen that most of the oil that is not evaporated enters the water column by the end of 20 days, leaving only a small residual amount on the surface.

Figure 7 shows the number of barrels on shore as a function of time. After 30 days only about 7% of the original spill has come on shore. A few barrels come ashore in the vicinity of Jubail Port after 9 or 10 days, and then a larger number comes ashore on the north coast of Bahrain and the off-lying reefs and on the tip of the Qatar peninsula during a 15–30 day period. Since only 7% of the spill comes ashore, one might be tempted to conclude that a spill of this magnitude in Marjan would not pose a significant threat to the coastline. However, this conclusion must be modified because, as it turns out, after 30 days there is a very considerable amount of oil dispersed in the water column in the regions immediately adjacent to the Qatar peninsula, and though this oil has not come ashore it is sufficiently close to pose a threat to some types of coastal and inshore installations and to inshore marine life.

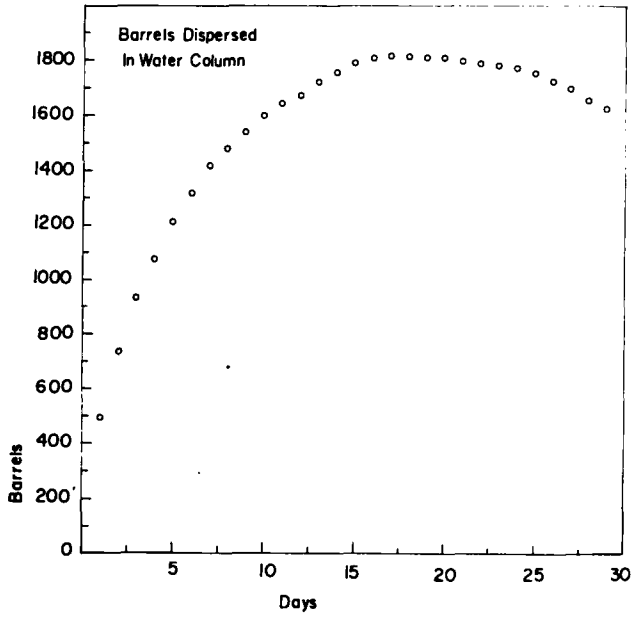

Figure 6 Number of barrels that have entered the water column as a function of time (days)

Figures 8–11 show the positions of the spill after 10 days at four levels of the water column. The contours represent lines of constant oil density, and the figures refer respectively to the density of the surface slick, the density between 0 and 10 m below the surface, the density between 10 and 20 m, and the density below 20 m. The initial spill site is indicated on each figure by a large cross. The surface slick is much more compact in the horizontal directions than the subsurface plume—a reflection of the divergence between the currents at different levels. The surface current sweeps the surface slick uniformly southeastward. However, once the oil disperses to the lower levels, the convective velocity is lower and at many points is reversed and sweeps the plume back toward the northwest. It can be seen that at this stage both the slick and the plume remain well offshore. The center of the slick has moved about 150 km from the spill site, but the subsurface plume stretches from the spill site for a distance of 200 km toward the southeast. After 30 days the positions of the slick and plume are shown in *Figures 12–15*. Relatively little oil remains on the surface at this stage. However, *Figure 13* shows that considerable amounts remain in the top 10 m of the water

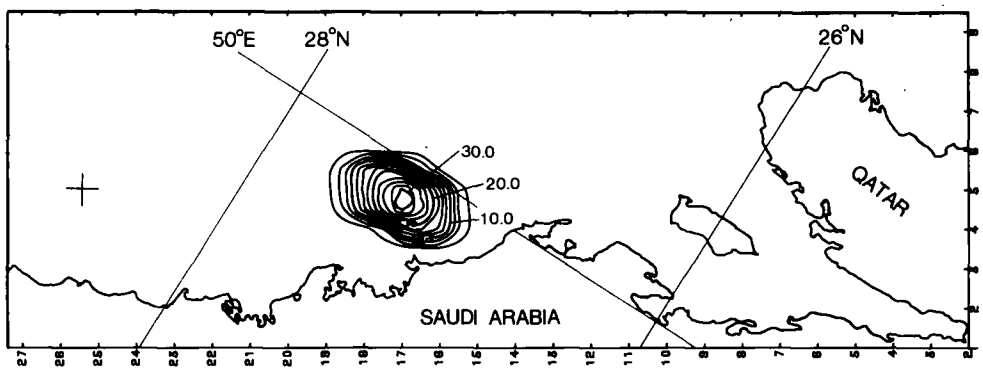

Figure 8 Contours of oil density on the surface after 10 days. Density is measured in the number of barrels per grid square (10 km × 10 km)

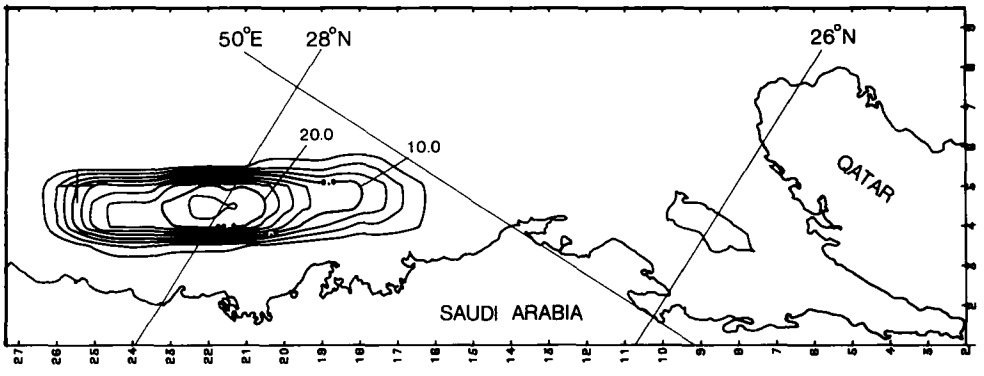

Figure 9 Contours of oil density between 0- and 10-m depth after 10 days

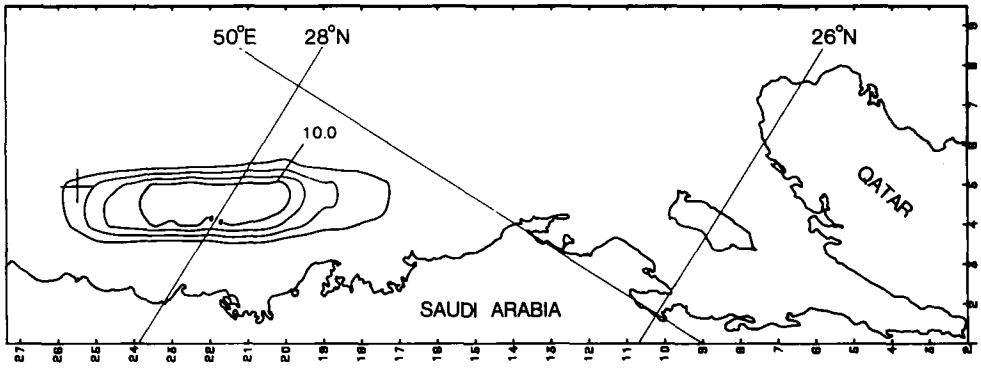

Figure 10 Contours of oil density between 10- and 20-m depth after 10 days

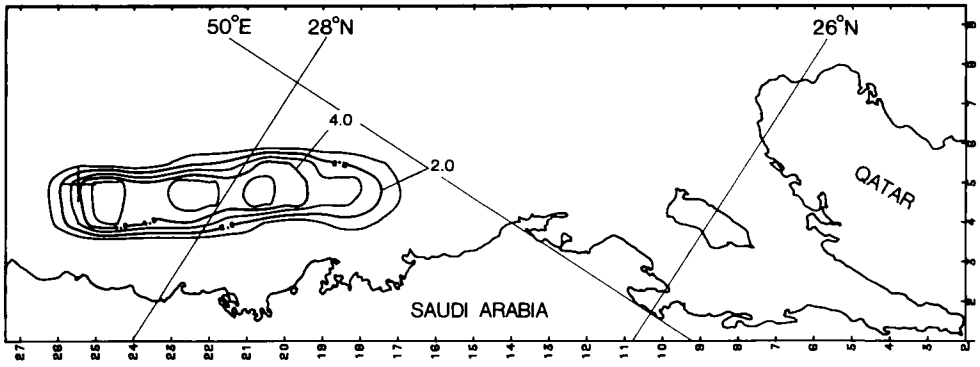

Figure 11 Contours of oil density below 20-m depth after 20 days

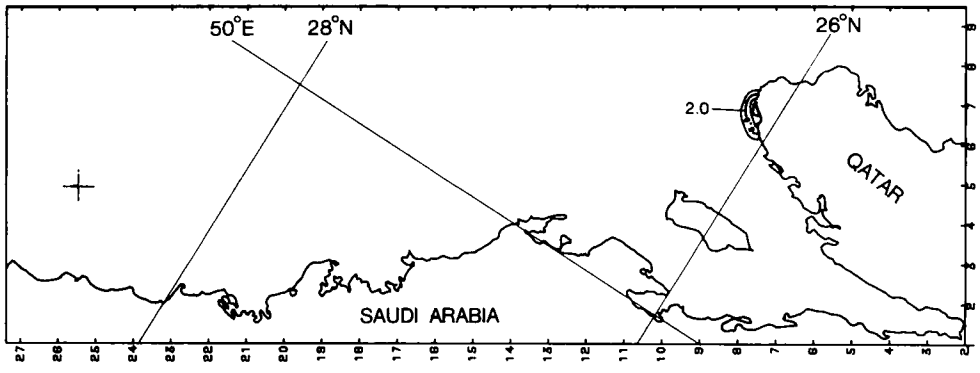

Figure 12 Contours of oil density on the surface after 30 days. Density is measured in the number of barrels per grid square (10 km × 10 km)

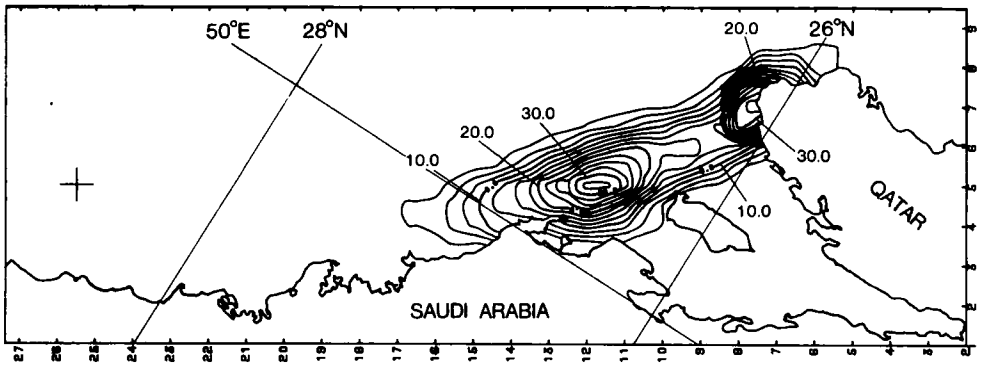

Figure 13 Contours of oil density between 0- and 10-m depth after 30 days

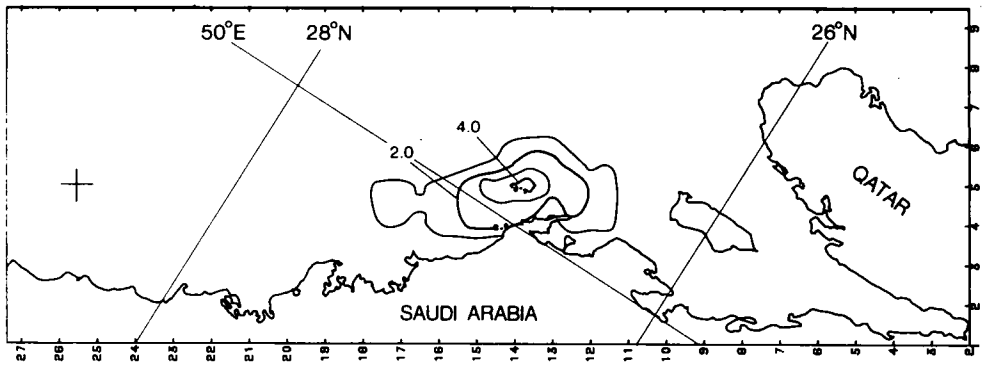

Figure 14 Contours of oil density between 10- and 20-m depth after 30 days

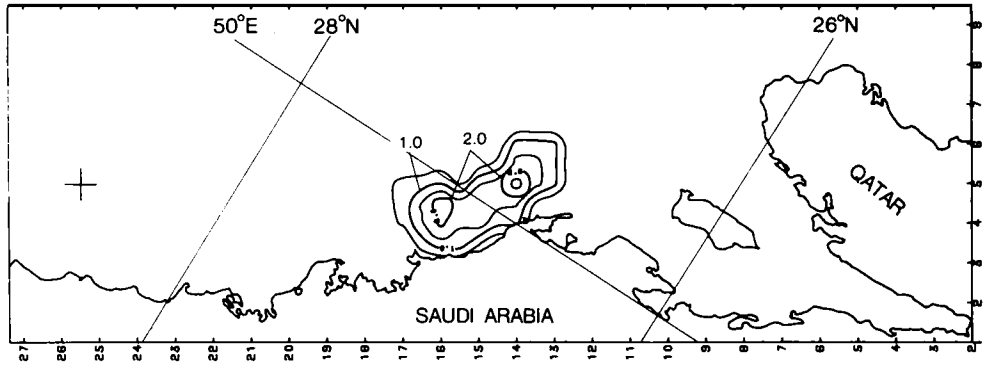

Figure 15 Contours of oil density below 20-m depth after 30 days

column, and at this stage much of this oil is close inshore. The area particularly threatened by this oil is the Qatar peninsula, with lesser densities of oil between Ras Tanura and Bahrain.

These figures indicate the type of prediction the model is capable of providing. The particular simulation described was run for annual average meteorological conditions. It would be equally possible to simulate a spill occurring under the average conditions of any month of the year. The location and size of spill as well as oil type could also be readily changed. However, it has not been considered necessary to present the results of more than one simulation in this paper.

References

1 Hughes, P. and Hunter, J. R. A proposal for a physical oceanography program and numerical modelling in the KAP region. Project of KAP 2/2, UNESCO, Paris, 1980

2 Hunter, J. R. The physical oceanography of the Arabian Gulf: A review and theoretical interpretation of previous observations, First Gulf Conference on Environment and Pollution, Kuwait, 1982

3 Galt, J. A., Payton, D. L., Torgrimson, G. M., and Watabayashi, G. Trajectory analysis for the Nowruz oil spill with specific applications to Kuwait, NOAA, Seattle, Wash., 1983

4 Lardner, R. W., Lehr, W. J., Fraga, R. J., and Sarhan, M. A. Residual circulation in the Arabian Gulf. I: Density-driven flow. *Arabian J. Sci. & Engg.* 1987, **12**, 341–354

5 Lardner, R. W., Lehr, W. J., Fraga, R. J., and Sarhan, M. A. Residual circulation in the Arabian Gulf. II: Wind-driven flow. *Arabian J. Sci. & Engg.* To be published

6 Lardner, R. W., Lehr, W. J., Fraga, R. J., and Sarhan, M. A. Thermally-driven circulation in the Arabian Gulf. To be published

7 MEPA. Preliminary report on drifting buoy movements. Ministry of Defense and Aviation, Jeddah, 1984

8 Hansen, W. Hydrodynamical methods applied to oceanographic problems. *Proc. Symp. Math. Hydrodyn. Phys. Ocean.*, Institüt für Meereskunde, Universität Hamburg, 1962, pp. 24–34

9 Leendertse, J. J. Aspects of a computational model for long period water-wave propagation. Rand Corp. Rep. RM-5294-PR, 1967

10 Lardner, R. W., Belen, M. S., and Cekirge, H. M. Finite difference model for tidal flows in the Arabian Gulf. *Comp. & Math. Applics.* 1982, **8**, 425–444

11 Lardner, R. W. and Cekirge, H. M. An efficient algorithm for the computation of three-dimensional wind-driven currents. *Engineering Analysis.* 1987, **4**, 89–94

12 Mathison, J. P. and Johansen, O. A numerical tidal and storm-surge model of the North Sea. *Marine Geodesy* 1983, **6**, 267–291

13 Lystad, M. and Martinsen, E. A. The importance of barotropic current for the simulation of oil spills. Norwegian Meteorol. Inst. Tech. Rep. No. 49, 1980

14 U.S. Navy. Climatic study of the Persian Gulf and Gulf of Oman. Naval Oceanography Command Detachment, Asheville, N.C., 1980

15 Neumann, G. and Pierson, W. J. *Principles of Physical Oceanography.* Prentice-Hall, 1964

16 Davies, A. M. On determining the profile of steady wind-induced currents. *Appl. Math. Modelling* 1985, **9**, 409–418

17 Golub, R. and Brus, E. Analysis of oil pollution in the Kuwait Action Plan Region. IMCO/UNEP Workshop on Combating Marine Pollution from Oil Exploration, Exploitation and Transport in the KAP Region, Dec. 6–10, 1980, Bahrain

18 Lehr, W., Cekirge, H., Fraga, R., and Belen, M. Empirical studies of the spreading of oil spills. *Oil Petrochemical Poll.* 1984, **2**, 7–11

19 Jeffrey, P. Large scale experiments on the spreading of oil at sea and its disappearance by natural factors. *Proceedings of the Joint Conference on Prevention and Control of Oil Spills*, Washington, D.C., 1973

20 Fay, J. Physical processes in the spread of oil on water surface. *Proceedings of Conference on Prevention and Control of Oil Spills*, API, Washington, D.C., 1970, pp. 463–467

21 Mackay, D. and Leinonen, P. Mathematical model of the behavior of oil spills on water with natural and chemical dispersion. Report No. EPS-3-EC-77-19 submitted to Environmental Protection Service, Canada, 1977

22 Lehr, W., Fraga, R., Belen, M., and Cekirge, H. A new technique to estimate initial spill size using a modified Fay-type spreading formula. *Marine Poll. Bull.* 1984, **15**, 326–329

23 Huang, J. A review of the state-of-the-art of oil spill fate/behavior models. *Proceedings of 1983 Oil Spill Conference*, 1983, pp. 313–323

24 Mackay, D. and Stiver, W. Testing of crude oil and petroleum products for environmental purposes. *Proceedings of 1983 Oil Spill Conference*, 1983, pp. 331–340

25 Holmes, P. *Proceedings Joint Conference on Prevention and Control of Oil Spills*, API, Washington, D.C., 1977

26 Blaikely, D., Dietzel, G., Glass, A., and van Kleef, P. *Proceedings Joint Conference on Prevention and Control of Oil Spills*, API, Washington, D.C., 1977

27 Aravamunden, K., Raj, P., Newman, E., and Tucker, W. Breakup of oil on rough seas; simplified model and step-by-step calculations. Report No. NTIS CG-D-69-79 prepared for United States Coast Guard, Washington, D.C., 1979

28 Okubo, A. Ocean diffusion diagrams. *Deep Sea Research* 1971, **18**, 789–802

29 Venkatesh, S., Sahota, H., and Rizkalla, A. *Proceedings of 1979 Oil Spill Conference*, API, Los Angeles, 1979

30 Nihoul, J. *Modelling of Marine Systems*. Elsevier, Amsterdam, 1975

31 Ahlstrom, S. A mathematical model for predicting the transport of oil slicks in marine waters, Battelle Laboratories, Richland, Washington, 1975

32 ARAMCO, Private communication